J Appl Electrochem (2014) 44:141–157
DOI 10.1007/s10800-013-0616-4

RESEARCH ARTICLE

Electrosorption on activated biochar: effect of thermo-chemical activation treatment on the electric double layer capacitance

Amir Mehdi Dehkhoda · Naoko Ellis · Előd Gyenge

Received: 17 April 2013 / Accepted: 13 August 2013 / Published online: 25 August 2013

Abstract Biochar, a by-product of woody biomass pyrolysis, is investigated as a renewable and low-cost carbon-based electrode material for electric double layer (EDL) applications. To increase the surface area and porosity of the biochar chemical (7 M KOH) and thermal (at 675 and 1,000 °C, respectively) activation treatments are applied. The thermo-chemically activated biochar samples are investigated by a combination of physico-chemical surface characterization and electrochemical methods to reveal the relationship between the activation process variables, the resulting porous carbon structural features and EDL capacitance. For electrochemical testing, the activated biochar is sprayed onto Ni mesh current collectors with or without Nafion® as binder. Based on cyclic voltammetry experiments in 0.1 M NaCl–0.1 M NaOH a maximum EDL capacitance of 167 F g^{-1} is obtained for the activated biochar electrode prepared at 675 °C. The latter capacitance is about 50 times higher than the EDL capacitance of a Vulcan XC-72 electrode prepared and tested under identical conditions. The activated biochar electrodes show also promising galvanostatic charge/discharge behavior and electrical conductivities up to 0.058 S cm^{-1} indicating suitability for EDL-type applications.

Keywords Electric double layer · Biochar · Thermo-chemical activation · Carbon electrode · Electrosorption · Capacitive deionization

1 Introduction

Among many different electrochemical applications that utilize carbon-based materials, those based on electric double layer (EDL) theory are of great interest for either energy storage (capacitors) or water treatment methods [electrosorption and capacitive deionization (CDI)] [1–9]. For capacitor applications carbon-based electrodes in various forms such as single and multi-wall nanotubes, graphene and aerogel, were proposed as promising energy storage materials with high capacitances (up to about 300 F g^{-1}) and long-term durability (e.g., thousands of charge–discharge cycles) [6, 7, 10–13]. Recently, Farma et al. [14] have prepared electrodes from fibers of oil palm fruit bunches to be used in supercapacitors. They have treated the raw biomass with KOH and CO_2 to produce highly porous carbon electrodes with surface area and pore volume up to 1,700 m^2 g^{-1} and 0.88 cm^3 g^{-1}, respectively. The maximum EDL capacity for the biomass-derived carbon electrodes was 150 F g^{-1} [14]. Their electrode preparation method involved a time, energy, and material consuming process including pre-carbonization and ball milling for 18 h prior to a simultaneous chemical and physical activation method using KOH and CO_2.

With respect to the other major EDL-based applications, electrosorption and CDI, are intensely studied as more sustainable, energy saving, and cost effective alternative water treatment technologies [5, 15, 16]. Electrosorption can be applied to remove a variety of heavy and transitional metal ions (e.g., Zn^{2+}, Cu^{2+}, Mn^{2+}, Cd^{2+}, and

Electronic supplementary material The online version of this article (doi:10.1007/s10800-013-0616-4) contains supplementary material, which is available to authorized users.

A. M. Dehkhoda · N. Ellis · E. Gyenge (✉)
Department of Chemical and Biological Engineering,
The University of British Columbia, 2360 East Mall, Vancouver,
BC V6T-1Z3, Canada
e-mail: egyenge@chbe.ubc.ca

$Cr^{3+,\ 6+}$) from their corresponding aqueous solutions or to purify water streams containing ions such as Na^+, Cl^-, Ca^{2+}, NO_3^-, usually referred to as CDI. Carbon-based electrodes of several compositional, structural and electrode configuration type were reported for both electrosorption and supercapacitor applications, including different activated carbon blacks, various carbon cloths, papers and felts, carbon nanotubes, carbon aerogels and graphene [10, 15, 17–27]. However, there still remains a chasm between performance and feasibility for practical implementation. In other words, some of the highest capacitance carbon electrodes might not be cost effective, especially for technologies that compete with more established non-electrochemical processes (e.g., in case of desalination); or carbons that may be cost effective, yet do not possess electrochemical characteristics superior to other technologies. In addition to the intrinsic physicochemical and structural properties of the carbons, the design of efficient EDL devices imposes engineering constraints such as high electrical conductivity of the porous carbon electrode, high solid–liquid mass transfer capacity, and low pressure drop for electrolyte flow.

Our research targets the value-added utilization of biochar and its potential applicability for CDI, electrosorption and supercapacitor fabrication. Biochar is one of the by-products of biomass pyrolysis having a low surface area (i.e., $<2\ m^2\ g^{-1}$) and a unique carbon structure. This material is categorized as a non-graphitic/non-graphitizable carbon having amorphous aromatic carbon sheets with turbostratic structure [28]. The edge area of each carbon sheet contains unsaturated carbon atoms having high concentrations of unpaired electrons playing an important role in adsorption [28, 29]. A high content of carbon–oxygen groups on the biochar surface can also be favorable for EDL application in terms of enhanced pseudo-capacitance [4].

Generally, in order to tailor the application-specific properties of carbons various chemical activation treatments have been developed [31–34]. With respect to biochar, to the knowledge of the authors, the cause and effect relationship involving pre-treatment activation variables, the resulting porous structural characteristics and the EDL capacitance has not been extensively explored. To contribute to this area, using biochar treated with 7 M KOH, here we report the effect of activation temperature (675 and 1,000 °C, respectively) on the structural features and EDL capacitance. The electrodes were prepared by spraying the activated powder biochar samples as an ink on Ni mesh current collector. Depositing the carbon material on a mechanically flexible, thin and electronically conductive metal mesh is advantageous, as it allows the fabrication of electrochemical cells with various configurations, such as stacked or rolled electrodes. To enhance the adherence of the activated biochar particles to the Ni mesh, the effect of Nafion® loading was also investigated. As electrolyte, 0.1 mol L^{-1} NaCl in 0.1 mol L^{-1} NaOH was employed. The results presented here are relevant to the CDI of alkaline NaCl solutions, which could have practical applicability for waste water treatment in the chlor-alkali industry.

2 Experimental section

2.1 Materials preparation

Biochar (generated from the fast pyrolysis of woody biomass) and Vulcan XC-72 (carbon black) materials were obtained from Dynamotive Energy Systems Corporation (Canada) and Cabot Corporation (US), respectively. Nafion® (5 wt% solution in a mixture of lower aliphatic alcohols and water) was purchased from Sigma-Aldrich Inc. and used as such. Iso-propanol (ACS reagent), HCl solution (37 wt% concentration), and HNO_3 (63 wt% concentration) were all purchased from Fisher Scientific. KOH pellets (>90 % purity) was purchased from Sigma-Aldrich. Acid-Resistant Nickel mesh (alloy 400 purchased from McMaster Carr with 150 × 150 mesh size per square inch) with 0.066 mm wire diameter was utilized as current collector.

2.1.1 Chemical activation of biochar samples

First, the dried biochar powder samples were mixed with a specific amount of 7 mol L^{-1} KOH solution such that the mass ratio of pure KOH to biochar was 3.55. After stirring this mixture at room temperature for 2 h in a beaker with a magnetic stirrer, the mixture was filtered and dried in an oven at 110 °C for 72 h. The dried KOH-treated samples were ground to powder using a ceramic mortar and pestle and placed in a tube furnace (Thermo Scientific Inc.) under nitrogen flow (258 mL min^{-1}). Two different activated biochar samples were produced using carbonization processes at different temperatures (675 and 1,000 °C, respectively). The samples were initially heated to 300 °C for 60 min. Afterward, one sample was heated to 675 °C for 2 h (dwell time); whereas, another sample was heated to 1,000 °C for 5 h (dwell time). The samples were then left to cool to room temperature under nitrogen flow followed by washing with distilled water until the pH of wash water became neutral. The washed samples were mixed with 250 mL of 0.1 mol L^{-1} HCl and stirred at room temperature for an hour for demineralization and complete removal of KOH. A final washing step was conducted after HCl treatment until the wash water became neutral. The treated and washed biochar was placed in oven for 24 h at

110 °C for drying. The activated biochar at 675 °C (with 2 h dwell time) and 1,000 °C (with 5 h dwell time) are referred to as Biochar-675 and Biochar-1000, respectively. These two activation conditions, i.e., 675 °C (with 2 h. dwell time) and 1,000 °C (with 5 h dwell time), were chosen based on literature in order to prepare and investigate biochar samples with high surface area according to Azargohar and Dalai [30], and more graphite-like structure [28], respectively.

2.1.2 Electrode preparation

Three types of electrodes were prepared and comparatively investigated: (i) as-received biochar (untreated); (ii) activated biochar (Biochar-675 and Biochar-1000, respectively); and (iii) as-received Vulcan XC-72 utilized as a reference carbon sample. The electrode preparation steps were the same for each carbon-based material. The carbon-based samples (i.e., untreated biochar, activated biochar, and Vulcan XC-72) were ground (using mortar and pestle) and sieved between 40 and 150 μm mesh sizes. The powder samples were then mixed with iso-propanol (99.9 % assay Fisher Scientific) and in some cases with Nafion® solution to prepare the ink composition for spraying onto the Ni mesh current collector. The ratio of iso-propanol volume to carbon mass was 0.25 mL mg^{-1}. For each carbon material, three different inks were produced based on increasing weight percentages of Nafion®, i.e., 0, 5, and 30 wt%. The prepared ink solutions were sonicated for 2 h and sprayed onto the Ni mesh current collector. The Ni mesh was placed on a heated (40 °C) and moving stainless steel plate controlled by computer numerical computation (CNC) and an IWATA air-brush was employed for homogeneous spraying. The Ni mesh was placed on a heated stainless steel plate (40 °C) to improve the spraying and prevent flooding of the mesh by the ink. The geometric area of the carbon-based electrodes on the Ni mesh current collector was 7.09 ± 0.35 cm^2. The carbon-based ink coating efficiency of the Ni mesh is summarized in Table 1.

2.2 Materials characterization

2.2.1 Physical and chemical characterization of the carbons

The total surface area (based on the Brunauer–Emmet–Teller (BET) model) and the micro- and meso-pore volumes (determined from the *t*-plot and Barrett, Joyner and Halenda (BJH) method, respectively) were determined using the nitrogen gas sorption technique on a Micromeritics ASAP 2020 Accelerated Surface Area and Porosimetry Analyzer. Before analysis, 0.2 g of each sample was vacuum degassed for 5–7 h in the built-in degas port of the instrument. The sum of the micro- and meso-pore volumes is referred to as the total pore volume for each sample.

Scanning electron microscopy (SEM) and Transmission electron microscopy (TEM) images of the carbon samples were taken using the Hitachi S3000N and Hitachi H7600 microscopes, respectively.

The carbon, oxygen, hydrogen, and nitrogen contents of the carbon-based samples were measured by Canadian Microanalytical Service, Ltd. (Delta, British Columbia). The elemental analysis of carbon, hydrogen, and nitrogen was performed by gas chromatography analysis of the combustion gases (CO_2, H_2O and N_2) obtained after exposing the carbon-based samples to oxygen flow at 1,800 °C. To measure the oxygen content of each sample, pyrolysis in the absence of air was done followed by measuring the CO content using gas chromatography.

Table 1 Prepared electrodes and coating efficiency of the Ni mesh current collector

Sample	Nafion® (wt%)	Total mass of coated material (mg)[a]	Mass of coated carbon-based material (mg)	Coating yield (%)[b]
Biochar-AR-0	0	8.2	8.2	5.1
Biochar-AR -5	5	15.9	15.1	12.5
Biochar-AR -30	30	13.9	9.7	24.2
Biochar-675-0	0	7.3	7.3	5.2
Biochar-675-5	5	18.9	17.9	8.9
Biochar-675-30	30	31.9	22.3	18.5
Biochar-1000-0	0	7.6	7.6	12.6
Biochar-1000-5	5	21	19.9	16.5
Biochar-1000-30	30	31.2	21.8	27.2
Vulcan-0	0	33.5	33.5	33.5
Vulcan-5	5	25.4	24.1	40.1
Vulcan-30	30	32.1	22.4	56

[a] Includes the carbon-based material and dry Nafion weight (where applicable)

[b] Coating yield = mass of carbon coated/total mass of carbon sprayed as ink solution

Table 2 Surface area and porosity

Sample	BET surface area ($m^2\ g^{-1}$)	Average pore size (nm)	*t*-plot micropore volume ($cm^3\ g^{-1}$)	BJH mesopore volume ($cm^3\ g^{-1}$)	Total pore volume ($cm^3\ g^{-1}$)
Biochar-AR	1.66	–	–	–	–
Biochar-675	990	3.20	0.31	0.59	0.90
Biochar-1000	614	3.88	0.03	0.63	0.66
Vulcan XC-72	200	5.05	0.03	0.31	0.34

About 100 mg of each sample was used for elemental analysis.

Surface functional groups were investigated using Fourier Transform Infra-Red (FT-IR) spectroscopy using a Varian 3100 FT-IR Excalibur Series spectrometer with attenuated total reflectance: Pike MIRacle^{TM}ATR with ZnSe crystal. Scan speed of 2.5 kHz with aperture setting of 4 cm^{-1} over a wave number range of 4,000–650 cm^{-1} were applied for spectra collection. For each sample 64 scans were co-added to improve the signal-to-noise ratio.

The crystallographic structure of each carbon-based sample was investigated using X-ray Diffraction analysis (XRD) on a Bruker AXS D8 Advance X-ray Diffractometer (in Bragg–Brentano configuration) equipped with a Lynxeye ID silicon strip detector. A Ni filter was used to strip out the Cu Kβ radiation thus leaving Cu Kα1,2 radiation generated at 40 kV and 40 mA. EVA 10.0.1.0 software was used for data interpretation.

2.2.2 *Electrochemical characterization*

A three-electrode cell at ambient temperature (22 °C) was employed for all electrochemical studies. A platinum mesh and mercury/mercury oxide electrode (Hg/HgO/KOH 0.1 mol L^{-1}) were used as counter and reference electrodes, respectively. All potentials in this work are reported versus the Hg/HgO/KOH 0.1 mol L^{-1} reference electrode. The electrolyte was composed of 0.1 mol L^{-1} NaCl in 0.1 mol L^{-1} NaOH. The working electrode was the carbon-deposited Ni mesh with a geometric area of 7.09 ± 0.35 cm^2.

The investigated electrodes were first electrochemically conditioned by performing 150 cycles at sweep rate of 50 mV s^{-1} between −0.536 to +0.464 V versus Hg/HgO, generating reproducible voltammograms. After the conditioning step, the EDL behavior of the electrodes was studied by cyclic voltammetry (CV) and charge/discharge experiments, respectively. The CV potential scanning was conducted at different sweep rates between 1 and 50 mV s^{-1} using the 1100A Series Electrochemical Analyzer (CH Instruments, USA).

Galvanostatic charge/discharge experiments were performed using the Solartron 1470E potentiostat. Constant currents (2 and −2 mA, respectively) were applied as charge and discharge currents at equal time intervals (varied between 10 and 100 s, respectively). The maximum potential was set to 0.55 V. The ohmic potential drop (IR-drop) of each electrode was also measured using the sudden drop of the potential while switching between the charging and discharging currents [13].

The electrical conductivity of carbon-based samples has been estimated by performing dry-cell polarization experiments. The dry activated biochar powder with particle sizes sieved between 40 and 150 μm mesh sizes, was added between two ultra-conductive Cu plates (alloy 101 McMaster-Carr) spaced at 2 mm and enclosed in a Plexiglas box. The polarization of the activated biochar powder was obtained by measuring the current–voltage dependence at room temperature. The experiments were repeated at least three times. The effective electrical conductivity of the dry activated biochar powder was calculated using Ohm's law after the correction for the contact resistance.

3 Results and discussion

3.1 Surface area, porosity, and morphology

One the most important characteristic of a promising carbon-based electrode in EDL-based applications is high surface area and porosity, with the caveat that micropores could be less useful due to overlapping EDLs [1, 7, 31]. In this study, as described in detail in the Sect. 2, we used chemical (i.e., KOH) activation combined with heat treatment, to develop the surface area and porosity of the biochar. The effect of the activation procedure on the surface area and porosity of the biochar is presented in Table 2. The activated biochar prepared at 675 °C with 2 h dwell time is referred to as Biochar-675, whereas the activated biochar prepared at 1,000 °C with 5 h dwell time is referred to as Biochar-1000. The detailed experimental procedure is described in the Sect. 2. Moreover, the surface area and porosity of Vulcan XC-72 were also measured and are shown for comparison (Table 2).

The as-received biochar material (referred to Biochar-AR from here on) has a very low surface area (<2 $m^2\ g^{-1}$)

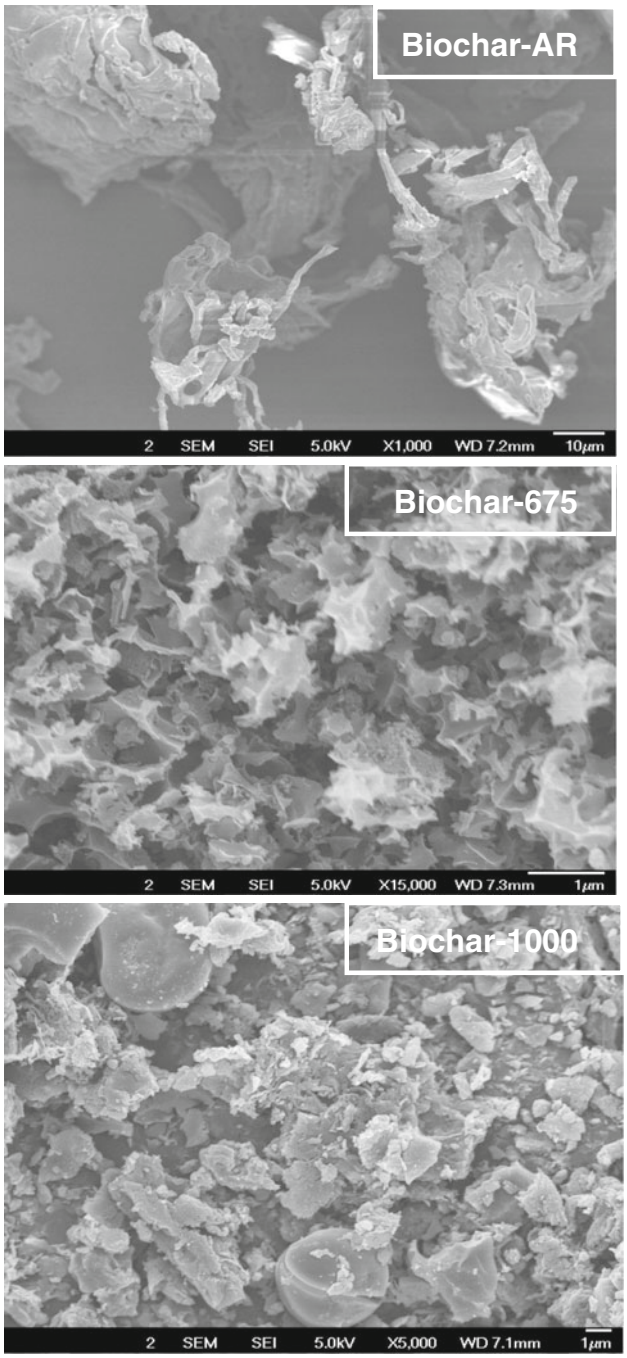

Fig. 1 SEM images of Biochar-AR, Biochar-675, and Biochar-1000 samples

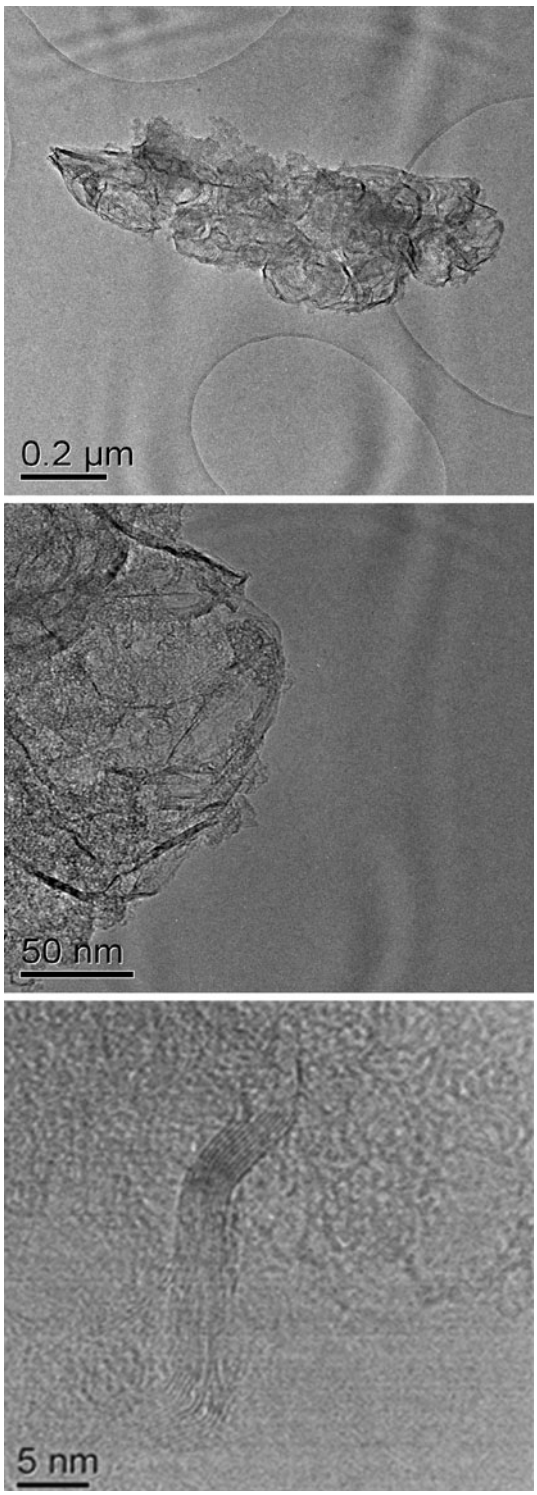

Fig. 2 TEM images of Biochar-1000

due to blockage of its pores (i.e., empty volumes between the crumpled and randomly cross-linked carbon sheets) by the tarry material evolved during the pyrolysis. The removal of tarry material through chemical activation with KOH increased the surface area and porosity of Biochar-AR as shown in Table 2. Moreover, the surface area and porosity of the activated biochar samples are considerably higher than that of Vulcan XC-72. The latter is well-known as an effective carbon material in a variety of electrochemical and EDL capacitive applications [31].

Comparing the surface areas of Biochar-675 to Biochar-1000, a significant decrease is observed with increasing the activation temperature and dwell time (Table 2). This can

Table 3 Elemental composition

Sample	C (wt%)	H (wt%)	N (wt%)	O (wt%)	H/C ratio	O/C ratio
Biochar-AR	63.36	2.41	<0.3	24.46	0.038	0.39
Biochar-675	80.62	0.87	<0.3	11.96	0.011	0.15
Biochar-1000	59.09	0.87	<0.3	5.16	0.015	0.087
Vulcan XC-72	97.39	<0.3	<0.3	0.63	<0.003	6.5×10^{-3}

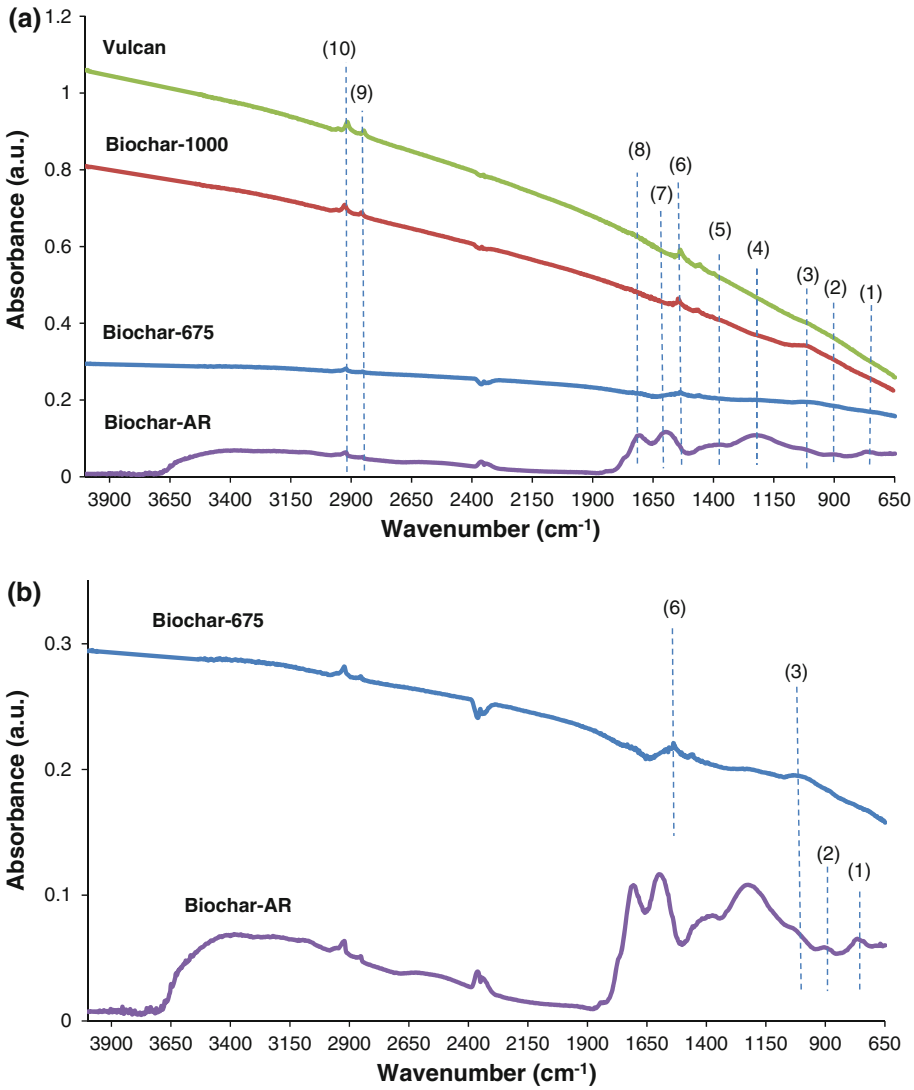

Fig. 3 FT-IR spectra of **a** all carbon-based samples; **b** Biochar-AR and Biochar-675 samples (peak numbers are used for better identification in Sect. 3)

be attributed to two phenomena: a potential collapse and burn-off of the micropore walls of biochar during higher activation temperature and longer dwell time, [32]; and/or, the development of localized graphite-like structure in the biochar matrix [33]. Distinguishing the total pore volume of Biochar-675 and Biochar-1000 as micropore and mesopore volumes, respectively, reveals a large differ ence between micropore content (0.31 vs. 0.03 $cm^3\ g^{-1}$), while showing almost similar mesopore volume (0.59 vs. 0.63 $cm^3\ g^{-1}$) (Table 2), further supporting the phenomenon of burn-off and collapse of micropore walls at high carbonization temperature and longer dwell time.

The surface morphology of Biochar-AR, Biochar-675, and Biochar-1000 were investigated using SEM (Fig. 1) and TEM (Fig. 2), respectively. Biochar-AR shows a disordered structure composed of large flakes, while the structures of both Biochar-675 and Biochar-1000 are more ordered composed of smaller flakes (Fig. 1). Furthermore, the TEM images in Fig. 2 show the presence of localized crystalline graphitic-type of structures in the Biochar-1000

sample. The TEM images of Biochar-675 did not reveal any crystalline structure formation at 675 °C (data not shown). These results confirm the phenomenon of developing more graphite-like structure within the biochar matrix by increasing the carbonization temperature and during longer dwell times [28, 34].

3.2 Elemental analysis

The C, H, O, and N elemental content of the investigated samples are presented in Table 3. Other residual elements such as K and Si are not detectable by the method employed, i.e., combustion (or pyrolysis) combined with gas chromatography (see in Sect. 2). These additional elements make up the weight percentage differences to 100 % in Table 3. According to the literature, biochar has a number of oxygen-containing functional groups such as carboxylic, phenolic, and lactone groups that contribute to physical adsorption and pseudo-capacitance [28]. This is confirmed here by the high weight percentage of oxygen in the as-received biochar sample (Biochar-AR). The chemical and thermal activation procedures employed to produce Biochar-675 and Biochar-1000, reduced the O/C and H/C weight ratios (Table 3) due to partial removal of oxygen and hydrogen, respectively.

3.3 FT-IR Spectroscopy

The surface functional groups of all carbon-based samples have been characterized by FT-IR spectroscopy (Fig. 3 a and b). The Biochar-AR showed a distinctive peak at 740–764 cm^{-1} (denoted as peak (1)), corresponding to the out-of-plane bending of ring C–H bonds of heteroatomic and aromatic compounds [28, 35] (Fig. 3b). Additional peaks at 910, 1020, 1210, and 1370 cm^{-1} (i.e., peaks (2), (3), (4), and (5)) are characteristic for O–H bend in carboxylic acid, C–O stretch in carboxylic acid, Ar–OH groups and C–H in alkanes, respectively. The peaks at 1,580 and 1,700 cm^{-1} (i.e., peaks (7) and (8) in Fig. 3a) are attributed to C–C stretch in ring mode and aromatic acidic groups [36]. Peaks around 2,300 cm^{-1} correspond to the adsorbed water in the analyzed sample; while peaks at 2,850 and 2,900 cm^{-1} (i.e., peaks (9) and (10)) are due to aromatic C–H bonds [36]. Finally, the broad peak in the 3,200–3,600 cm^{-1} region is assigned to phenolic OH groups.

Comparing the Biochar-AR and Biochar-675 spectra (Fig. 3a, b), the peaks at 740–764, 1210, 1370, 1580, and 1700 cm^{-1} (i.e., peaks (1), (4), (5), (7), and (8)) are either absent or weak in the Biochar-675 sample. This shows the removal of some of the heteroatoms during the thermo-chemical activation procedure in accordance also with the Elemental Analysis (Table 3). The extra peak at 1,530 cm^{-1} (i.e., peak (6)) in the Biochar-675 spectra is attributed to the development of additional C=C bonds within the carbon sheets as a result of chemical activation in Biochar-675 versus Biochar-AR [28].

The Biochar-1000 and Vulcan samples showed very similar spectra except for the presence of a small bump at 1,020 cm^{-1} (i.e., peak (3) Fig. 3a) in the former sample characterizing the presence of C=O bonds in carboxylic acid.

Comparing the Biochar-1000 and Biochar-675 spectra (Fig. 3) the more pronounced peaks at 1530, 2850, and 2900 cm^{-1} in case of Biochar-1000 is indicative of higher content of C=C and C–H aromatic bonds confirming the development of more graphite-like structures as shown also in TEM images (Fig. 2).

These results suggest that the surface functional groups and the structure of Biochar-AR were changed significantly via the activation procedure mainly through removal of heteroatoms and development of graphite-like structures. The Biochar-675 sample has more oxygen-containing groups in the form of carboxylic and phenolic groups as compared to Biochar-1000 and Vulcan samples, which could be potentially favorable for EDL applications by

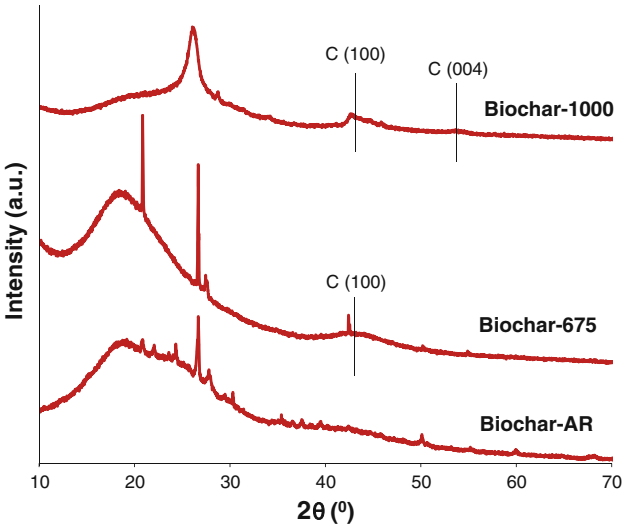

Fig. 4 XRD patterns of biochar electrodes

Table 4 Electrical conductivity

Sample	Electrical conductivity (S cm^{-1})
Biochar-AR	7.0×10^{-9}
Biochar-675	6.74×10^{-3}
Biochar-1000	5.80×10^{-2}
Vulcan XC-72	2.70×10^{-1}

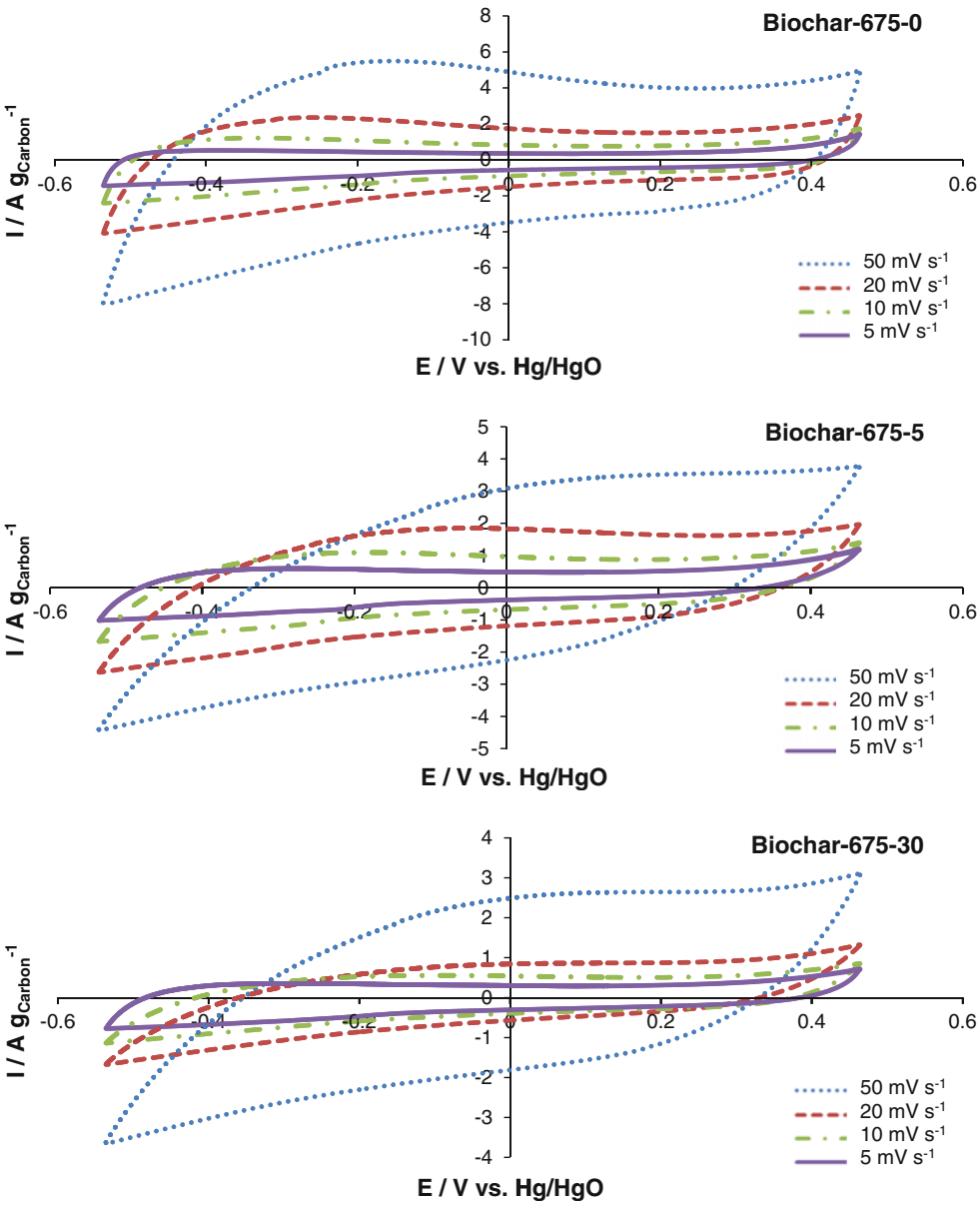

Fig. 5 CV diagrams of Biochar-675 electrodes at different sweep rates with 0, 5, and 30 wt% Nafion content using 0.1 mol L^{-1} NaCl in 0.1 mol L^{-1} NaOH electrolyte

increasing the pseudocapacitance and wettability of the electrode.

3.4 XRD analysis

The structural changes among the as-received (AR) and activated biochar samples (Biochar-675 and Biochar-1000, respectively) were further investigated by XRD analyses (Fig. 4). In case of Biochar-AR, the broad peak in the region of $2\theta = 15$–$30°$ is indexed as C(002) diffraction peak indicating amorphous carbon structure with randomly oriented aromatic sheets. Sharp peaks around $2\theta = 21°$, 22°, 26°, 30.5°, and 49° correspond to the miscellaneous inorganic components mainly constituted of quartz, within the structure of Biochar-AR [37, 38]. Additional sharp peaks at $2\theta = 24°$ and 37° can also be indexed as whewellite [$Ca(C_2O_4)\cdot H_2O$] compounds [38], while further peaks at $2\theta = 36°$ and 39° can be attributed to calcite compounds [37, 38]. Thus, these various peaks correspond to the ash content and tarry materials trapped within the pores of the as-received biochar sample. In the case of the biochar sample treated at 675 °C many of these peaks have been eliminated or significantly reduced, thereby, confirming the removal of the majority of ash content. Moreover, for Biochar-675 the broad C(002) peak in the region of $2\theta = 15$–$30°$ became narrower and another broad diffraction peak corresponding to graphite C(100) at $2\theta = 40$–$50°$ is apparent (Fig. 4). The latter peak is typically observed in ordered turbostratic carbon crystallites [34, 35, 39, 40]. Comparing the XRD spectra of Biochar-675 and Biochar-1000, the peaks between

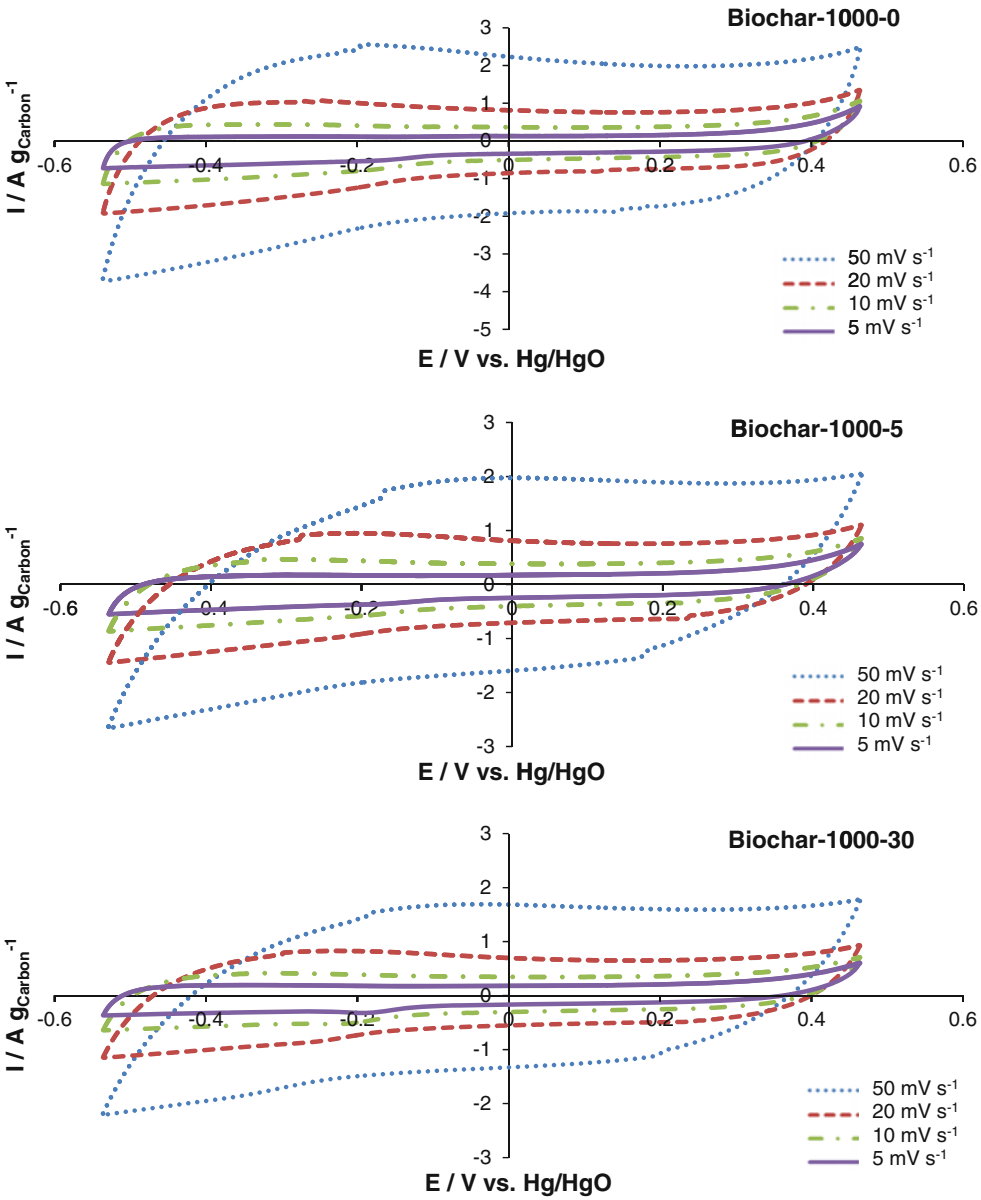

Fig. 6 CV diagrams of Biochar-1000 electrodes at different sweep rates with 0, 5, and 30 wt% Nafion content using 0.1 mol L^{-1} NaCl in 0.1 mol L^{-1} NaOH electrolyte

$2\theta = 15$–$30°$ and $2\theta = 40$–$50°$ are narrower for the latter (Fig. 4), confirming the formation of more graphite-like structure at the higher activation temperature as previously shown also by the TEM and FT-IR results (Figs. 2, 3).

3.5 Electrochemical characterization

3.5.1 Electrical conductivity

One of the important characteristics of a promising electrode material is electrical conductivity. The electrical conductivity of carbon materials is strongly dependant on the content of heteroatoms, hybridization, thermal treatment, and microstructure [7]. Additionally, other variables are also influencing the electrical conductivity of carbonaceous powders including the shape and size of grains, porosity, and the amount of compression applied in the cell [41].

Table 4 summarizes the measured electric conductivities of the powder biochar carbon-based samples. The Vulcan sample has also been tested in the same setup because it is a commonly used material in electrochemical applications. Comparing Biochar-AR with Biochar-675 and Biochar-1000, respectively, the electrical conductivity increased significantly with thermo-chemical activation. Moreover, the Biochar-1000 sample showed almost an order of magnitude higher electrical conductivity than Biochar-675 (Table 4). This can be attributed to the generation of more graphite-like structure along with lower

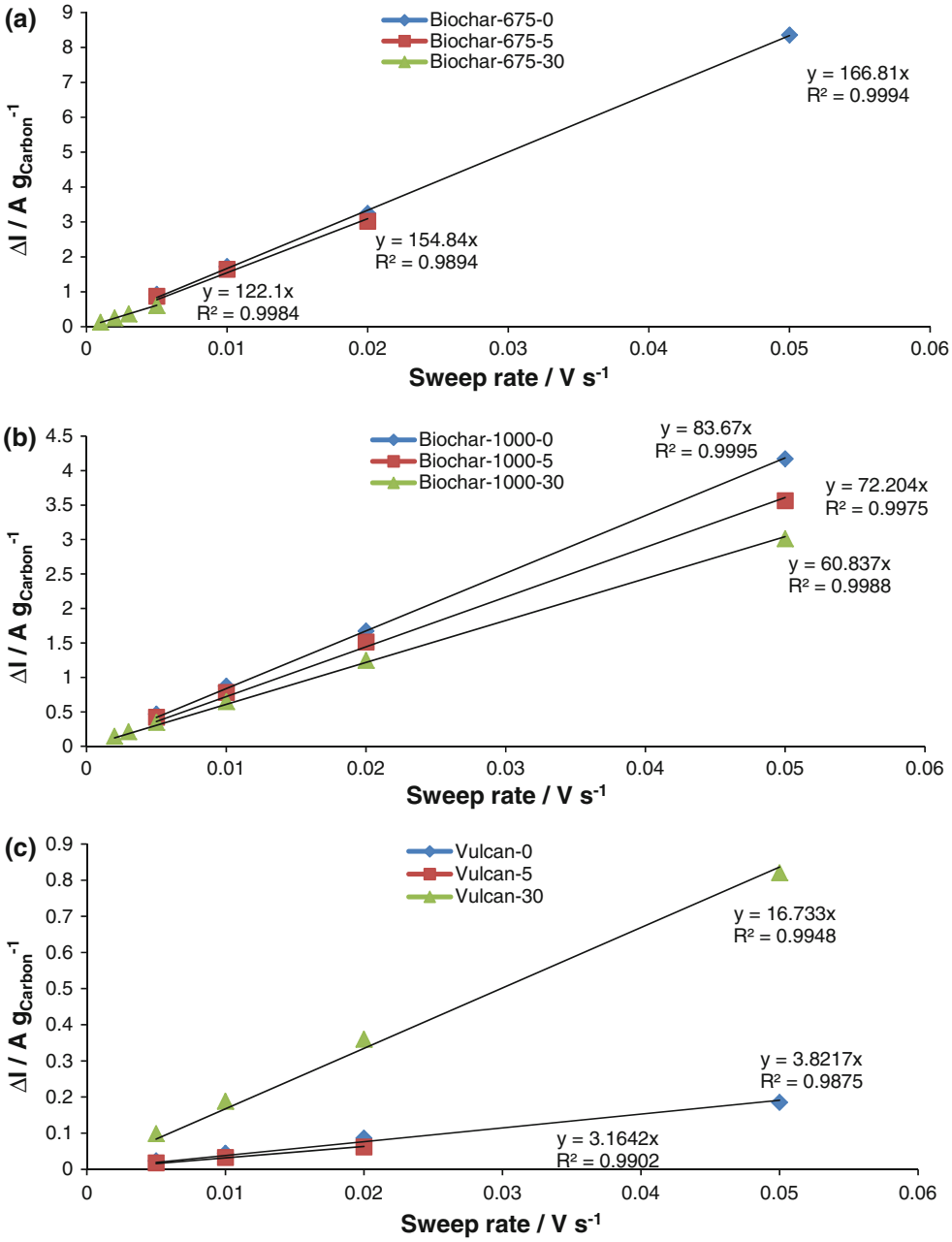

Fig. 7 Current difference ($\Delta I = I_a - |I_c|$) at 0 V versus Hg/HgO as a function of sweep rates for: **a** Biochar-675; **b** Biochar-1000; and **c** Vulcan electrodes. Electrolyte: 0.1 mol L^{-1} NaCl in 0.1 mol L^{-1} NaOH

content of heteroatoms (as evidenced by Sect. 3.2, TEM images, FT-IR, and XRD results) resulting in fewer barriers for electrons to be transferred within microcrystalline units [35, 42].

3.5.2 *Cyclic voltammetry (CV)*

Using each carbon-based material under investigation (i.e., as-received biochar (Biochar-AR), activated biochars (Biochar-675 and Biochar-1000, respectively) and Vulcan XC-72 (for comparison)), electrodes were prepared by spraying on the Ni mesh current collectors. The prepared electrodes contained 0, 5, or 30 wt% of Nafion® as binder. The carbon-based ink and the electrode preparation procedure involving spraying of the carbon-Nafion ink on a Ni mesh current collector are described in detail in the Sect. 2. Increasing the amount of Nafion® mixed with the carbon improved the attachment of the carbon particles to the current collector as reflected by the increased carbon coating yield (Table 1). The Nafion® content of each electrode in wt% is referred to in the last digit of electrode's name, e.g., Biochar-AR-0 and Biochar-675-5 refers to biochar electrodes prepared using as-received biochar and activated biochar (at 675 °C and 2 h dwell time) with 0 and 5 wt% Nafion®, respectively.

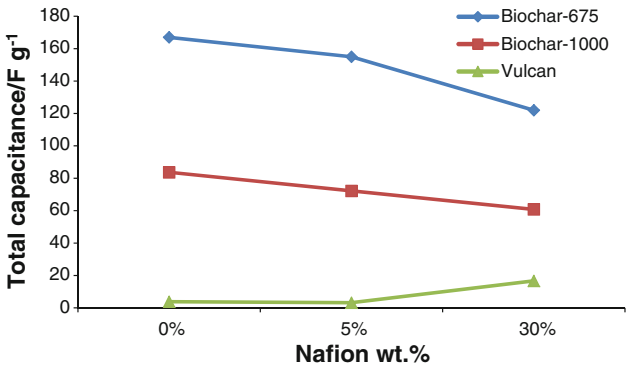

Fig. 8 Total capacitance per unit mass of carbon versus Nafion® content for the two activated biochar electrodes and Vulcan XC-72. Electrolyte: 0.1 mol L^{-1} NaCl in 0.1 mol L^{-1} NaOH

Table 5 Normalized capacitance per mesopore volume of biochar electrodes

Electrode	Total capacitance per mesopore volume (F cm^{-3})
Biochar-675-0	282
Biochar-675-5	261
Biochar-675-30	207
Biochar-1000-0	133
Biochar-1000-5	114
Biochar-1000-30	95.9

CV experiments of the activated biochar and Vulcan XC-72 electrodes was conducted in a three-electrode set-up using 0.1 mol L^{-1} NaCl in 0.1 mol L^{-1} NaOH as electrolyte at different potential sweep rates ranging between 1 and 50 mV s^{-1}. The CV of the pure Ni mesh current collector was also recorded (data not shown) to offset any potential contributions to the current generated by the carbon electrodes. The contribution of the Ni mesh was found to be negligible in the explored potential range (e.g., at 50 mV s^{-1} the current was lower than 0.2 mA). Furthermore, the Biochar-AR electrodes (i.e., as-received without thermo-chemical activation) showed virtually negligible EDL behavior as expected based on the very low surface area (i.e., 1.66 m^2 g^{-1}, Table 2). Hence, the activated biochar electrodes, Biochar-675 and Biochar-1000, respectively, were studied in detail and compared to the Vulcan XC-72 electrodes (Figs. 6, 7). The CV diagrams for the Vulcan electrodes show typical EDL behavior between −0.5 and +0.5 V versus Hg/HgO with one reduction wave between −0.2 and −0.4 V corresponding to the reduction of oxygen-containing functional groups such as ketone and quinone groups as well as reduction of the dissolved oxygen in the electrolyte (see Fig. 1 in Online Resource) [31, 43].

The CV behavior of the electrodes prepared with Biochar-675 with three different Nafion contents (i.e., Biochar-675-0, Biochar-675-5, and Biochar-675-30) is shown in Fig. 5. The voltammograms obtained at slower sweep rates (<10 mV s^{-1}) have a shape that is closer to the ideal EDL capacitive response (i.e., more rectangular-like), hence, confirming similar reports in the literature [27, 44, 45]. This can be mostly attributed to the longer time available for ions to access the micropore content of Biochar-675 (Table 2) at slower sweep rates. Panić et al. [31] reported a similar observation in their study using a carbon-black electrode. The addition of 5 and 30 wt% Nafion® to Biochar-675 resulted in some shape deformation of the voltammograms at faster sweep rates (e.g., 20 and 50 mV s^{-1}). The Nafion loading could hamper the access of ions to the carbon surface sites and also it could lower the electrical conductivity among the carbon particles (see further).

The electrodes prepared with Biochar-1000 revealed also typical EDL behavior in CV tests (Fig. 6). However, two differences are noted when comparing the voltammograms of Biochar-1000 and Biochar-675 electrodes (Figs. 6, 5, respectively). First, the Biochar-1000 voltammograms are somewhat more rectangular in shape (i.e., closer to the ideal capacitive EDL behavior) particularly at high sweep rates (such as 20, and 50 mV s^{-1}), and second, the addition of Nafion (5 and 30 wt%) caused minimal shape distortion in case of Biochar-1000. The high mesopore content and negligible micropore content of Biochar-1000 compared to Biochar-675 (Table 2) is beneficial because the mesopores are less prone to blockage by Nafion agglomerates (micelles). Comparing the activated biochar voltammograms with that of Vulcan (see Fig. 1 in Online Resource), it can be observed that the reduction peak of the oxygen-containing functional groups is absent in the case of the biochar samples. This can be due to the different type of oxygen-containing groups (e.g., phenolic and carboxylic) in the biochar samples as opposed to the Vulcan sample (containing quinone-type functional groups that are involved in the redox catalysis of O_2 reduction).

The total capacitance of an electrode can be quantified using the cyclic voltammogram by dividing the anodic and cathodic current differences ($(\Delta I = I_a - |I_c|)$ at the EDL plateau region with the corresponding sweep rate [13, 27, 46]. Thus, plotting the current differences obtained from Figs. 5 and 6 at the plateau of each CV (i.e., at 0 V) versus the potential sweep rate should yield a linear function, with the slope representing the total capacitance per unit carbon mass of each investigated electrode (Fig. 7). For all electrodes the current difference at 0 V versus potential sweep

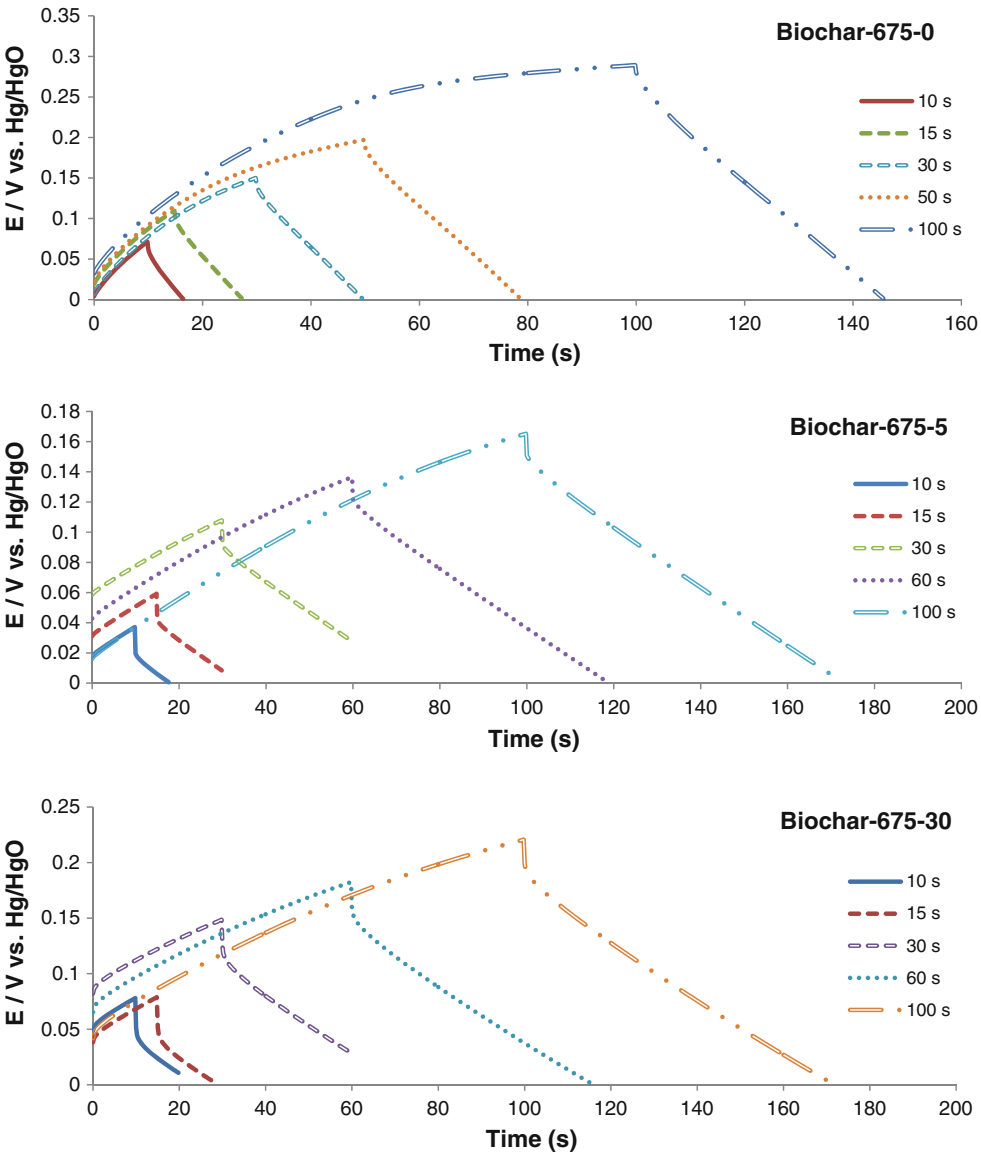

Fig. 9 Galvanostatic charge/discharge of Biochar-675 electrodes using +2 and −2 mA charge and discharge currents, respectively. Electrolyte: 0.1 mol L^{-1} NaCl in 0.1 mol L^{-1} NaOH

rate showed excellent linear fit, allowing therefore, the calculation of the total capacitance as a function of carbon material and Nafion content (Fig. 7).

As presented in Fig. 8, increasing the Nafion® content in Biochar-675 electrodes from 0 to 30 wt% (i.e., from Biochar-675-0 to Biochar-675-30) resulted in a decrease of the total capacitance from 167 to 122 F g^{-1}. The Biochar-1000 electrodes showed a similar trend of decreased total capacitance with increasing Nafion® content, albeit the Biochar-1000 electrodes have a lower total capacity than Biochar-675. The Vulcan electrodes revealed significantly smaller total capacitance (between 3.16 and 16.7 F g^{-1}) than any of the activated biochar samples. These results support the proposal of using biochar-based electrodes in EDL-based applications.

In order to further investigate the role of micropores and mesopores on the capacitive behavior of biochar-based electrodes, the total capacitance of the electrodes presented in Fig. 8 were normalized by the respective total mesopore volumes given in Table 2. The results are shown in Table 5.

The mesopore volumes of Biochar-675 and 1000 electrodes are very similar, 0.59 and 0.63 cm^3 g^{-1}, respectively (Table 2). However, Table 5 shows the total capacitance per mesopore volume of the Biochar-675 electrode is more than two times higher than the total capacitance of the Biochar-1000 electrode. This finding could be rationalized by considering two phenomena: (i) the higher micropore content of Biochar-675 (Table 2) could provide additional useful surface area for EDL formation in spite of the possibility of EDL overlap; (ii) the higher content of oxygen-containing functional groups in Biochar-675 (as shown in Sect. 3.2, Table 3, and FT-IR results, Fig. 3) could also contribute to the total

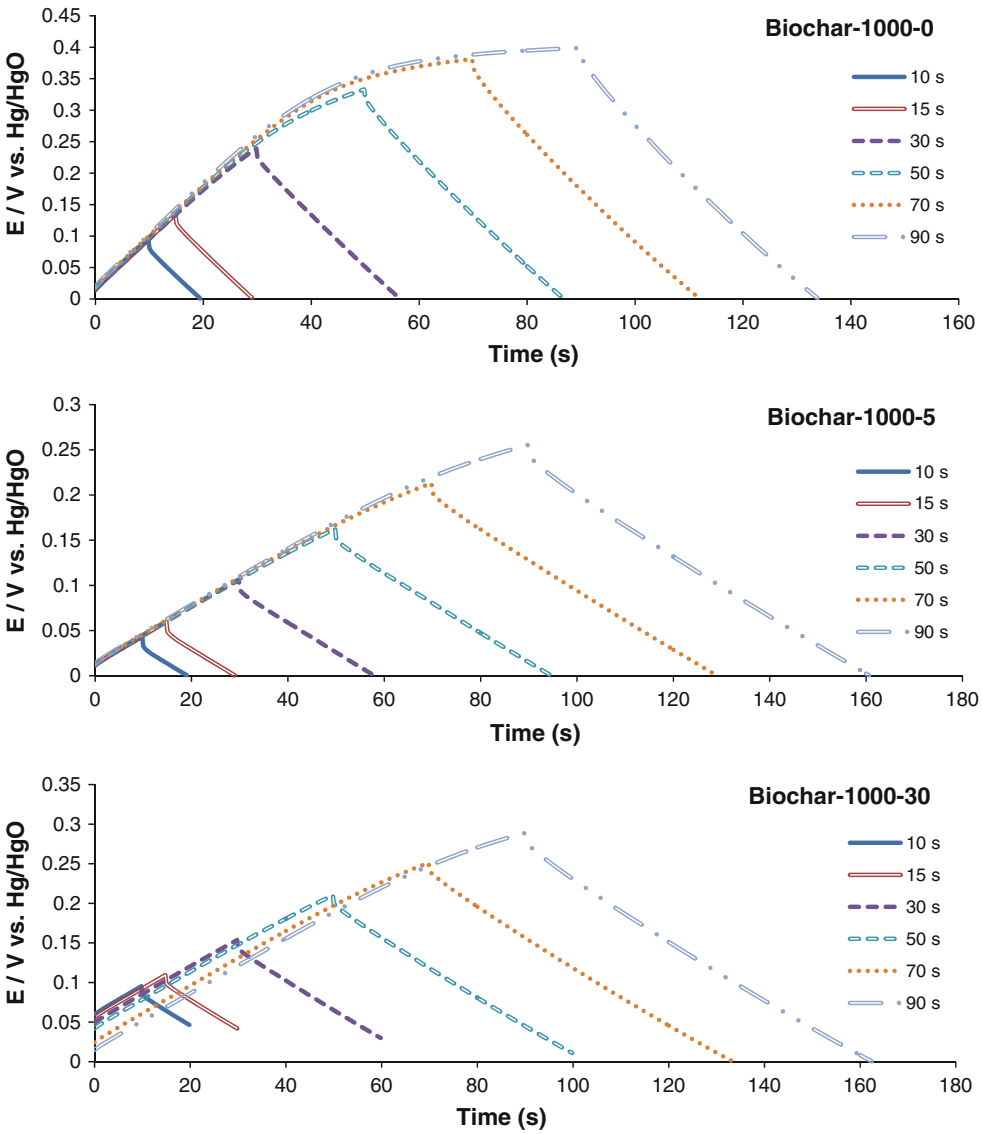

Fig. 10 Galvanostatic charge/discharge of Biochar-1000 electrodes using +2 and −2 mA charge and discharge currents, respectively. Electrolyte: 0.1 mol L^{-1} NaCl in 0.1 mol L^{-1} NaOH

capacitance in the form of pseudo-capacitance and increased wettability [7].

3.5.3 Galvanostatic charge/discharge analysis

In EDL-based processes, both the adsorption and desorption of ions from the electrode surface are essential. Figures 9 and 10 show the galvanostatic charge/discharge profiles of the activated biochars as a function of the Nafion content, while Fig. 11 shows the galvanostatic charge/discharge profile of the reference Vulcan XC-72 electrode.

The sudden potential drop while switching the charging current to discharge current is the ohmic potential drop (or IR-drop). The ohmic potential drop of each electrode was measured from the potential difference between the last point on the charging curve and the first point on the discharge curve. This is essentially an application of the current interrupt method for ohmic drop measurement [13, 45].

Table 6 shows the ohmic potential drops associated with each of the investigated electrodes. The ohmic potential drop of the Biochar-675 electrodes increased from 0.009 to 0.025 V with increase of the Nafion® content from 0 to 30 wt%. At the highest Nafion loading, the polymer electrolyte film formed in the highly microporous Biochar-675 sample imposes a high ohmic drop (0.025 V). For the Biochar-1000 electrodes, characterized by very low micropore content (Table 2), the ohmic potential drop is virtually independent of the Nafion content. Moreover, with the exception of the 30 wt% Nafion Biochar-675 electrode, the ohmic potential drops for all the activated biochar electrodes are very similar to that of Vulcan electrodes.

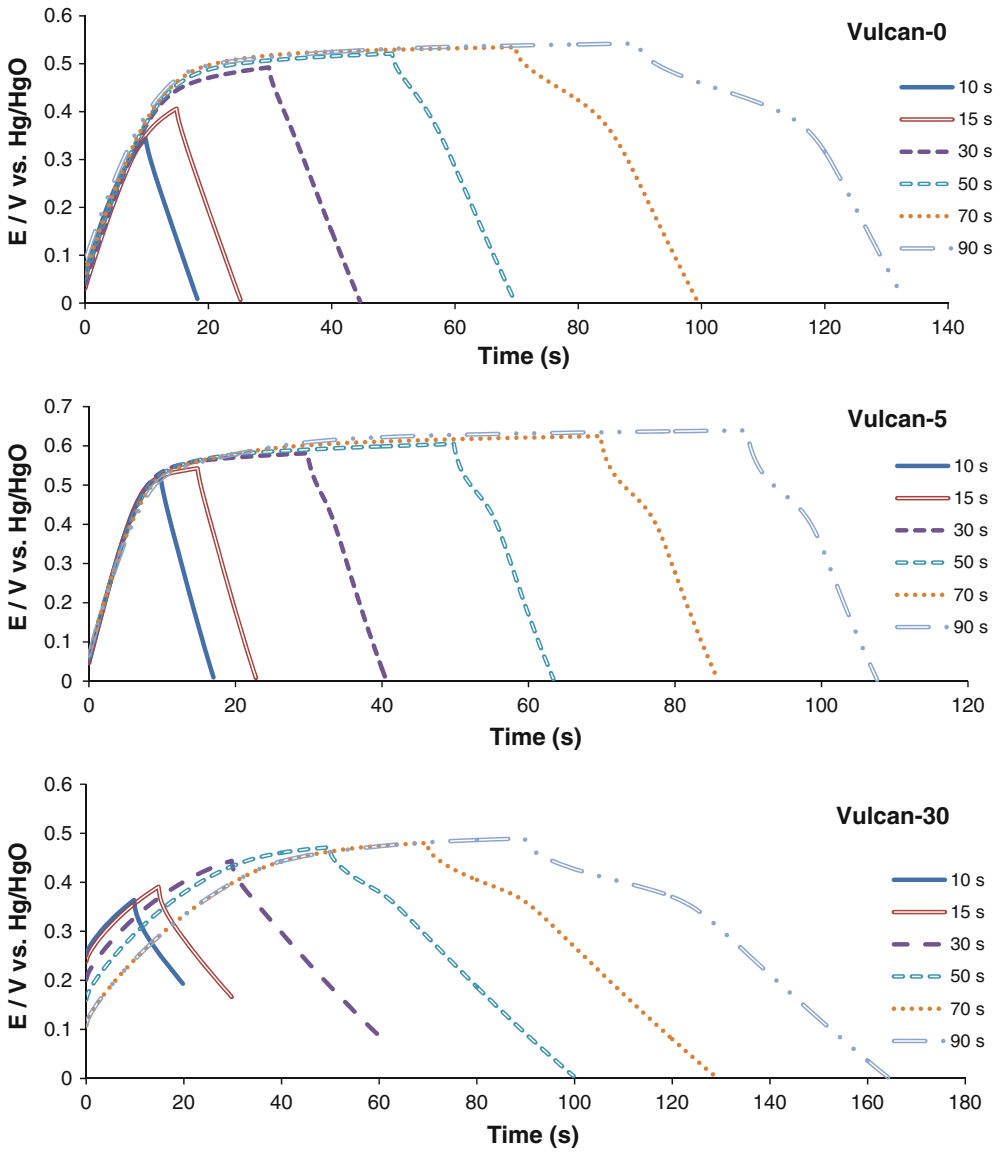

Fig. 11 Galvanostatic charge/discharge of Vulcan electrodes using +2 and −2 mA charge and discharge currents, respectively. Electrolyte: 0.1 mol L^{-1} NaCl in 0.1 mol L^{-1} NaOH

Table 6 The ohmic potential drop and discharge capacitance of the carbon electrodes calculated from the galvanostatic charge/discharge profiles

Electrode	Ohmic potential drop (V)	Discharge capacitance (F g^{-1})
Biochar-675-0	0.009	42.1
Biochar-675-5	0.016	55.4
Biochar-675-30	0.025	33.2
Biochar-1000-0	0.013	31.5
Biochar-1000-5	0.010	30.6
Biochar-1000-30	0.010	24.6
Vulcan-0	0.014	1.8
Vulcan-5	0.019	1.4
Vulcan-30	0.012	8.3

The discharge capacitance of each electrode has been calculated by multiplying the $\Delta t/\Delta E$ term obtained from the linear section of the discharge portion of the galvanostatic charge/discharge diagrams (Figs. 9, 10, 11) with the discharge current of −2 mA. The resultant values were then normalized per mass of carbon-based material used to fabricate the electrode. As shown in Table 6, the discharge capacitances of all the prepared electrodes follow the same trend as the total capacitance obtained from CV (Table 5). The discharge capacitances at −2 mA for Biochar-675 and Biochar-1000 electrodes were significantly higher (up to thirty-times higher) than those of Vulcan-based electrodes (Table 6). A direct comparison with other carbon-based electrodes reported in the literature is difficult due to

Table 7 Summary and comparison of the electric double layer total capacitances of the activated biochar electrodes and other relevant carbon-based electrodes

Electrode type	Total capacitance ($F\ g^{-1}$)	Electrolyte	Reference
Biochar-675	122–167	0.1 M NaCl in 0.1 M NaOH	–
Biochar-1000	60.8–83.6		
Vulcan XC-72	3.16–16.7		
Single-wall carbon nanotube on carbon cloth (CNTs/CC)	190–210	0.5 M Na_2SO_4	[44]
Graphene- PEDOT[a]	116–304	2 M HCl	[27]
Activated carbon cloth	41.5	'Hard' water	[16]
Multi-walled carbon nano tube	10–15	1.96 M $TEMABF_4$	[48]
Carbon aerogel	95	1 M H_2SO_4	[49]
Modified carbon aerogel with Ru	206		
Activated carbon from fibers of oil palm fruit bunches	150	1 M H_2SO_4	[14]

[a] Polyethylenedioxythiophene

different electrode preparation and test conditions utilized. Nevertheless, the reported typical ranges of discharge capacitances for other carbon-based electrodes are 23 $F\ g^{-1}$ for carbon aerogel, 19 $F\ g^{-1}$ for activated carbon, and 10 $F\ g^{-1}$ for carbon-black electrodes [47]. Hence, based on Table 6 the activated biochar electrodes with discharge capacitances between 24.6 and 42.1 $F\ g^{-1}$ compare favorably to other carbon electrodes reported in the literature.

4 Conclusion

Activated biochar electrodes were prepared and their EDL behavior was investigated by CV and galvanostatic charge/discharge experiments. The as-received biochar material (Biochar-AR) was chemically activated with 7 mol L^{-1} KOH and thermally treated at 675 °C (Biochar-675) and 1,000 °C (Biochar-1000), respectively. As a result of the chemical and thermal treatment, the surface area of the biochar increased from 1.66 $m^2\ g^{-1}$ (as-received biochar) up to 990 $m^2\ g^{-1}$, and the porosity increased as well from virtually negligible (for the as-received sample) up to 0.9 $cm^3\ g^{-1}$. Furthermore, the chemical and thermal activation (Biochar-675 and Biochar-1000) caused the removal of heteroatoms and tarry materials evidenced by Elemental Analyses, FT-IR, and XRD results.

XRD, TEM, and electrical conductivity analyses suggested more graphite-like structure and higher electrical conductivity for Biochar-1000 compared to Biochar-675. Electrodes were fabricated and investigated for EDL application using the two types of activated biochar samples exposed to 0.1 mol L^{-1} NaCl–0.1 mol L^{-1} NaOH electrolyte. The electrode fabrication method included spraying of the carbon-based inks on Ni mesh using Nafion® as binder. The Nafion content of the electrodes was between 0 and 30 wt% and the corresponding effect on the EDL performance was also investigated. CV and galvanostatic charge/discharge experiments confirmed unequivocally the potential of these novel electrodes to be employed in EDL-related applications. The total capacitance of the activated biochar electrodes measured by CV analysis was up to about 50 times higher than that of Vulcan electrodes prepared by the same technique (Table 7). Furthermore, the total capacitances of the biochar electrodes are also competitive with much more expensive systems such as CNTs and graphene-based electrodes (Table 7). These results suggest that activated biochars are promising, low-cost and renewable candidates for EDL-based applications including electrosorption, CDI, and supercapacitors. Moreover, the value-added utilization of biochar would increase the overall economic outlook of woody biomass pyrolysis. In future work, the activated biochar electrodes should be investigated in a variety of electrolytes such as H_2SO_4, Na_2SO_4, ionic liquids, etc. Furthermore, the design of the activated biochar electrodes should be optimized for selected target applications such as removal of toxic ions from waste water streams or supercapacitor fabrication. Each of these applications require specific electrochemical engineering design features that were beyond the objectives of the present work.

Acknowledgments The authors acknowledge the generous financial support of the Natural Sciences and Engineering Research Council of Canada (NSERC) Discovery and Discovery Accelerator Supplement Grant program and Rio Tinto Alcan Inc. in the form of the Graduate Student Award to Amir Mehdi Dehkhoda.

References

1. Yang K-L, Ying T-Y, Yiacoumi S et al (2001) Electrosorption of ions from aqueous solutions by carbon aerogel: an electrical

double-layer model. Langmuir 17:1961–1969. doi:10.1021/la001527s
2. Wang G, Qian B, Dong Q et al (2013) Highly mesoporous activated carbon electrode for capacitive deionization. Sep Purif Technol 103:216–221. doi:10.1016/j.seppur.2012.10.041
3. Ghosh A, Lee YH (2012) Carbon-based electrochemical capacitors. ChemSusChem 5:480–499. doi:10.1002/cssc.201100645
4. Hulicova-Jurcakova D, Fiset E, Lu GQM, Bandosz TJ (2012) Changes in surface chemistry of carbon materials upon electrochemical measurements and their effects on capacitance in acidic and neutral electrolytes. ChemSusChem 5:2188–2199. doi:10.1002/cssc.201200376
5. Foo KY, Hameed BH (2009) A short review of activated carbon assisted electrosorption process: an overview, current stage and future prospects. J Hazard Mater 170:552–559. doi:10.1016/j.jhazmat.2009.05.057
6. Oren Y (2008) Capacitive deionization (CDI) for desalination and water treatment—past, present and future (a review). Desalination 228:10–29. doi:10.1016/j.desal.2007.08.005
7. Frackowiak E, Béguin F (2001) Carbon materials for the electrochemical storage of energy in capacitors. Carbon 39:937–950. doi:10.1016/S0008-6223(00)00183-4
8. Salitra G, Soffer A, Eliad L et al (2000) Carbon electrodes for double-layer capacitors I. Relations between ion and pore dimensions. J Electrochem Soc 147:2486–2493. doi:10.1149/1.1393557
9. Noked M, Avraham E, Soffer A, Aurbach D (2009) The rate-determining step of electroadsorption processes into nanoporous carbon electrodes related to water desalination. J Phys Chem C 113:21319–21327. doi:10.1021/jp905987j
10. Gao Y, Pan L, Li H et al (2009) Electrosorption behavior of cations with carbon nanotubes and carbon nanofibres composite film electrodes. Thin Solid Films 517:1616–1619. doi:10.1016/j.tsf.2008.09.065
11. Dai H, Wong EW, Lieber CM (1996) Probing electrical transport in nanomaterials: conductivity of individual carbon nanotubes. Science 272:523–526. doi:10.1126/science.272.5261.523
12. Kim YJ, Yang C-M, Park KC et al (2012) Edge-enriched, porous carbon-based, high energy density supercapacitors for hybrid electric vehicles. ChemSusChem 5:535–541. doi:10.1002/cssc.201100511
13. Mitra S, Sampath S (2004) Electrochemical Capacitors Based on Exfoliated Graphite Electrodes. Electrochem Solid State Lett 7:A264–A268. doi:10.1149/1.1773752
14. Farma R, Deraman M, Awitdrus A et al (2013) Preparation of highly porous binderless activated carbon electrodes from fibres of oil palm empty fruit bunches for application in supercapacitors. Bioresour Technol 132:254–261. doi:10.1016/j.biortech.2013.01.044
15. Farmer JC, Bahowick SM, Harrar JE et al (1997) Electrosorption of chromium ions on carbon aerogel electrodes as a means of remediating ground water. Energy Fuels 11:337–347. doi:10.1021/ef9601374
16. Seo S-J, Jeon H, Lee JK et al (2010) Investigation on removal of hardness ions by capacitive deionization (CDI) for water softening applications. Water Res 44:2267–2275. doi:10.1016/j.watres.2009.10.020
17. Ayranci E, Conway BE (2001) Adsorption and electrosorption of ethyl xanthate and thiocyanate anions at high-area carbon-cloth electrodes studied by in situ UV spectroscopy: development of procedures for wastewater purification. Anal Chem 73:1181–1189. doi:10.1021/ac000736e
18. Yang C-M, Choi W-H, Na B-K et al (2005) Capacitive deionization of NaCl solution with carbon aerogel-silicagel composite electrodes. Desalination 174:125–133. doi:10.1016/j.desal.2004.09.006
19. Corry B (2008) Designing carbon nanotube membranes for efficient water desalination. J Phys Chem B 112:1427–1434. doi:10.1021/jp709845u
20. Oren Y, Soffer A (1978) Electrochemical parametric pumping. J Electrochem Soc 125:869–875. doi:10.1149/1.2131570
21. Gabelich CJ, Tran TD, Suffet IH "Mel" (2002) Electrosorption of inorganic salts from aqueous solution using carbon aerogels. Environ Sci Technol 36:3010–3019. doi: 10.1021/es0112745
22. Ban A, Schafer A, Wendt H (1998) Fundamentals of electrosorption on activated carbon for wastewater treatment of industrial effluents. J Appl Electrochem 157:602–615. doi:10.1023/A:1003247229049
23. Dai K, Shi L, Fang J et al (2005) NaCl adsorption in multi-walled carbon nanotubes. Mater Lett 59:1989–1992. doi:10.1016/j.matlet.2005.01.042
24. Farmer JC, Mack GV, Fix DV (1996) The Use of Carbon Aerogel Electrodes for Deionizing Water and Treating Aqueous Process Wastes. P 4th Int Congr Environ Conscious Des Manuf
25. Zou L, Morris G, Qi D (2008) Using activated carbon electrode in electrosorptive deionisation of brackish water. Desalination 225:329–340. doi:10.1016/j.desal.2007.07.014
26. Ghodbane I, Hamdaoui O (2008) Removal of mercury(II) from aqueous media using eucalyptus bark: kinetic and equilibrium studies. J Hazard Mater 160:301–309. doi:10.1016/j.jhazmat.2008.02.116
27. Alvi F, Ram MK, Basnayaka PA et al (2011) Graphene–polyethylenedioxythiophene conducting polymer nanocomposite based supercapacitor. Electrochim Acta 56:9406–9412. doi:10.1016/j.electacta.2011.08.024
28. Lehmann J, Joseph S (2009) Biochar for environmental management. Earthscan, London
29. Marsh H, Heintz EA, Rodríguez-Reinoso F (1997) Introduction to carbon technologies. University of Alicante Publications, Alicante
30. Azargohar R, Dalai AK (2008) Steam and KOH activation of biochar: experimental and modeling studies. Microporous Mesoporous Mater 110:413–421. doi:10.1016/j.micromeso.2007.06.047
31. Panić VV, Stevanović RM, Jovanović VM, Dekanski AB (2008) Electrochemical and capacitive properties of thin-layer carbon black electrodes. J Power Sources 181:186–192. doi:10.1016/j.jpowsour.2008.03.048
32. Bansal RC, Goyal M (2005) Activated carbon adsorption. CRC Press, Boca Raton
33. Patrick JW (1995) Porosity in carbons: characterization and applications. Halsted Press, Sydney
34. Franklin RE (1951) Crystallite growth in graphitizing and non-graphitizing carbons. Proc Roy Soc Lond Ser A 209:196–218
35. Yu JT, Dehkhoda AM, Ellis N (2011) Development of biochar-based catalyst for transesterification of canola oil. Energy Fuels 25:337–344. doi:10.1021/ef100977d
36. Brewer CE, Schmidt-Rohr K, Satrio JA, Brown RC (2009) Characterization of biochar from fast pyrolysis and gasification systems. Environ Prog Sustain Energy 28:386–396. doi:10.1002/ep.10378
37. Sun K, Ro K, Guo M et al (2011) Sorption of bisphenol A, 17α-ethinyl estradiol and phenanthrene on thermally and hydrothermally produced biochars. Bioresour Technol 102:5757–5763. doi:10.1016/j.biortech.2011.03.038
38. Singh B, Singh BP, Cowie AL (2010) Characterisation and evaluation of biochars for their application as a soil amendment. Aust J Soil Res 48:516–525
39. Azargohar R, Dalai A (2006) Biochar as a precursor of activated carbon. Appl Biochem Biotech 131:762–773. doi:10.1385/ABAB:131:1:762
40. Keiluweit M, Nico PS, Johnson MG, Kleber M (2010) Dynamic molecular structure of plant biomass-derived black carbon

(biochar). Environ Sci Technol 44:1247–1253. doi:10.1021/es9031419
41. Celzard A, Mareche J, Payot F, Furdin G (2002) Electrical conductivity of carbonaceous powders. Carbon 40:2801–2815. doi:10.1016/S0008-6223(02)00196-3
42. Pandolfo AG, Hollenkamp AF (2006) Carbon properties and their role in supercapacitors. J Power Sources 157:11–27. doi:16/j.jpowsour.2006.02.065
43. Wei ZD, Yan C, Tan Y et al (2008) Spontaneous reduction of Pt(IV) onto the sidewalls of functionalized multiwalled carbon nanotubes as catalysts for oxygen reduction reaction in PEMFCs. J Phys Chem C 112:2671–2677. doi:10.1021/jp709936p
44. Hsu Y-K, Chen Y-C, Lin Y-G et al (2012) High-cell-voltage supercapacitor of carbon nanotube/carbon cloth operating in neutral aqueous solution. J Mater Chem 22:3383. doi:10.1039/c1jm14716a
45. Wang G, Ling Y, Qian F et al (2011) Enhanced capacitance in partially exfoliated multi-walled carbon nanotubes. J Power Sources 196:5209–5214. doi:10.1016/j.jpowsour.2011.02.019
46. Bao L, Zang J, Li X (2011) Flexible Zn_2SnO_4/MnO_2 core/shell nanocable−carbon microfiber hybrid composites for high-performance supercapacitor electrodes. Nano Lett 11:1215–1220. doi:10.1021/nl104205s
47. Zhao Y, Zheng M, Cao J et al (2008) Easy synthesis of ordered meso/macroporous carbon monolith for use as electrode in electrochemical capacitors. Mater Lett 62:548–551. doi:16/j.matlet.2007.06.002
48. Honda Y, Haramoto T, Takeshige M et al (2007) Aligned MWCNT sheet electrodes prepared by transfer methodology providing high-power capacitor performance. Electrochem Solid State Lett 10:A106–A110. doi:10.1149/1.2437665
49. Miller JM, Dunn B, Tran TD, Pekala RW (1997) Deposition of ruthenium nanoparticles on carbon aerogels for high energy density supercapacitor electrodes. J Electrochem Soc 144:L309–L311. doi:10.1149/1.1838142